Journal of Virological Methods 272 (2019) 113701

Contents lists available at ScienceDirect

Journal of Virological Methods

journal homepage: www.elsevier.com/locate/jviromet

A strand-specific real-time quantitative RT-PCR assay for distinguishing the genomic and antigenomic RNAs of Rift Valley fever phlebovirus

Breanna Tercero[a], Kaori Terasaki[a,b], Keisuke Nakagawa[a], Krishna Narayanan[a], Shinji Makino[a,b,c,d,e,*]

[a] Departments of Microbiology and Immunology, The University of Texas Medical Branch, Galveston, TX 77555-1019, United States
[b] Institute of Human Infection and Immunity, The University of Texas Medical Branch, Galveston, TX 77555-1019, United States
[c] Center for Biodefense and Emerging Infectious Diseases, The University of Texas Medical Branch, Galveston, TX 77555-1019, United States
[d] UTMB Center for Tropical Diseases, The University of Texas Medical Branch, Galveston, TX 77555-1019, United States
[e] The Sealy Institute for Vaccine Sciences, The University of Texas Medical Branch, Galveston, TX 77555-1019, United States

ARTICLE INFO

Keywords:
Rift Valley fever phlebovirus
Strand-specific quantitative PCR
RNA replication

ABSTRACT

Rift Valley Fever phlebovirus (RVFV), genus *Phlebovirus*, family *Phenuiviridae*, order *Bunyavirales,* has a single-stranded, negative-sense RNA genome, consisting of L, M and S segments. Here, we report the establishment of a strand-specific, quantitative reverse transcription (RT)-PCR assay system that can selectively distinguish between the genomic and antigenomic RNAs of each of the three viral RNA segments produced in RVFV-infected cells. To circumvent the obstacle of primer-independent cDNA synthesis during RT, we used a tagged, strand-specific RT primer, carrying a non-viral 'tag' sequence at the 5' end, which ensured the strand-specificity through the selective amplification of only the tagged cDNA in the real-time PCR assay. We used this assay system to examine the kinetics of intracellular accumulation of genomic and antigenomic viral RNAs in mammalian cells infected with the MP-12 strain of RVFV. The genomic RNA copy numbers, for all three viral RNA segments, were higher than that of their corresponding antigenomic RNAs throughout the time-course of infection, with a notable exception, wherein the M segment genomic and antigenomic RNAs exhibited similar copy numbers at specific times post-infection. Overall, this assay system could be a useful tool to gain an insight into the mechanisms of RNA replication and packaging in RVFV.

1. Introduction

Viruses belonging to the Order *Bunyavirales* carry segmented RNA genomes that can cause serious and important diseases in both human and domestic animals. Rift Valley fever phlebovirus (RVFV), a member of the genus *Phlebovirus,* family *Phenuiviridae*, order *Bunyavirales,* is a mosquito-borne virus that can cause severe disease in humans and ruminants. RVFV is endemic in sub-Saharan Africa but has spread to Madagascar and the Arabian Peninsula (Balkhy and Memish, 2003; Linthicum et al., 2016; Madani et al., 2003; Pepin et al., 2010). Human infection occurs from the bite of infected mosquitos or from direct transmission of the virus from infected animal tissues or blood. Human disease manifestations include transient incapacitating febrile illness, encephalitis, vision loss and hemorrhagic fever(Al-Hazmi et al., 2005; Alrajhi et al., 2004; Deutman and Klomp, 1981; Ikegami and Makino, 2011; Linthicum et al., 2016; Pepin et al., 2010; Peters et al., 1989). RVFV has the potential to spread to any area of the world, including North America, by naturally occurring mosquito populations (Gargan et al., 1988; House et al., 1992; Linthicum et al., 2016; Rolin et al., 2013). One of the hallmarks of diseases caused by RVFV is high mortality in young ruminants and high rates of abortion in pregnant animals called "abortion storms" causing an enormous negative impact on the economy of affected regions. The lack of anti-viral treatments and licensed vaccines for use in humans or domestic animals is of great concern.

RVFV carries three genomic RNA segments, L, M, and S (Fig. 1). L and M segments are of negative-sense polarity, whereas S segment is of ambisense polarity. The RNA genome segments are encapsidated by the nucleocapsid protein, N, and also bound to the L protein, the RNA-dependent RNA polymerase, forming the ribonucleoprotein (RNP) complexes. In virus-infected cells, three different viral RNA species are produced for each of the three viral RNA segments, which include the

* Corresponding author at: Department of Microbiology and Immunology, The University of Texas Medical Branch, 4.142E Medical Research Building, 301 University Boulevard, Galveston, TX 77555-1019, United States.
E-mail address: shmakino@utmb.edu (S. Makino).

https://doi.org/10.1016/j.jviromet.2019.113701
Received 13 May 2019; Accepted 13 July 2019
Available online 14 July 2019

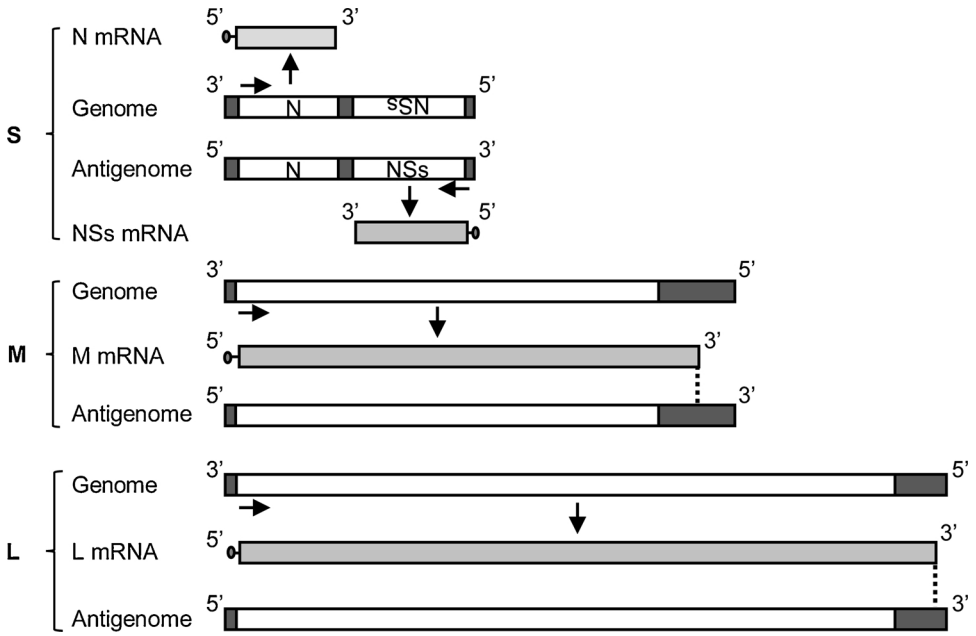

Fig. 1. RVFV RNA species and coding strategy. Schematic showing all RNA species for each viral segment. Full length genomic segments are negative sense and serve as templates for the generation of complementary antigenomic RNAs. The S segment has an ambisense coding strategy wherein, the N mRNA is transcribed from the genomic RNA and NSs mRNA is transcribed from the antigenomic RNA. The genomic strands of L and M segments are used as templates to generate L and M mRNAs, respectively. The dashed lines indicate the 3'-ends of L and M mRNAs compared to the full-length antigenomic segments.

genomic RNA, its complementary antigenomic RNA and cognate mRNAs. Immediately after infection, the incoming genomic L and M RNAs serve as templates for the synthesis of their respective antigenomic RNAs and mRNAs. The L mRNA encodes L protein and the M mRNA encodes two accessory proteins, NSm and the 78-kDa protein, along with two major envelope glycoproteins, Gn and Gc. The RVFV S segment uses an ambisense strategy for gene expression. The incoming genomic S RNA serves as the template for the synthesis of N mRNA encoding the N protein, while antigenomic S RNA serves as the template for the synthesis of NSs mRNA, which encodes NSs, a non-structural protein, which is a major viral virulence factor (Bouloy and Weber, 2010; Gaudreault et al., 2019; Gauliard et al., 2006; Hornak et al., 2016; Ikegami, 2012; Ikegami and Makino, 2011; Sun et al., 2018). A host-derived cap structure is added to the 5'-end of all viral mRNAs by a cap-snatching mechanism, but viral mRNAs lack the poly (A) sequence at the 3'-end (Hopkins and Cherry, 2013). The three viral RNA segments have noncoding regions (NCRs) that flank the open reading frames (ORFs). In the antigenomic sense, L, M and S segments have a relatively shorter 5' NCRs than their 3' NCRs, which vary in length, including 107 nt for L RNA, 271 nt for M RNA and 34 nt for S RNA. These NCRs carry signals necessary for viral RNA synthesis and viral RNA packaging (Gauliard et al., 2006; Murakami et al., 2012). The 3' NCRs of antigenomic L segment and M segment also carry transcription termination signals for L mRNA and M mRNA, respectively. The S segment carries an intergenic NCR, which harbors the transcription termination signals for N and NSs mRNAs, between the N and NSs ORFs (Albarino et al., 2007; Ikegami et al., 2007; Lara et al., 2011).

An insight into the underlying rules and mechanisms that drive viral RNA replication is valuable for understanding the regulation of virus replication and the pathogenic potential of the virus. This knowledge is also critical for the development of antiviral drugs and the design of strategies for live attenuated vaccines. Although it is well-established that L and N proteins drive viral RNA synthesis in the cytoplasm of cells infected with bunyaviruses(Bouloy and Weber, 2010; Gaudreault et al., 2019; Hornak et al., 2016; Ikegami, 2012; Ikegami and Makino, 2011; Sun et al., 2018), our knowledge about the mechanisms of bunyavirus RNA replication is limited. In fact, due to the absence of an assay system that can accurately distinguish between genomic and antigenomic viral RNA segments, the accumulation kinetics of replicating viral RNA segments and their relative abundance during infection have not been reported for any bunyaviruses. A lack of such an assay system has also hindered the advancement of our knowledge about other aspects of the viral replication cycle, for example, clarifying the mechanism of viral RNA packaging into virus particles.

In this study, we have developed a strand-specific RT-qPCR assay that accurately distinguishes between the genomic and antigenomic RNAs of RVFV L, M and S segments. Using this assay system, we examined the accumulation kinetics of the genomic and antigenomic viral RNAs in RVFV-infected cells. Our study represents the first quantitative analysis of the kinetics of intracellular accumulation of genomic and antigenomic viral RNA segments in bunyaviruses.

2. Materials and methods

2.1. Cell culture and virus infection

Vero E6 cells (kidney epithelial cells from African green monkeys) were cultured in Dulbecco's Modified Eagle Medium (DMEM), supplemented with 5% fetal bovine serum (FBS) and 1% penicillin-streptomycin. Huh7 cells (human hepatocellular carcinoma cells) were cultured in DMEM supplemented with 10% FBS and 1% kanamycin. RVFV MP-12 strain was generated by a reverse genetics system (Ikegami et al., 2006) and passaged once in Vero E6 cells. The virus titers were determined by plaque assay in Vero E6 cells. For virus infection, Vero E6 and Huh7 cells, with 90% confluency in 6-well plates, were inoculated with MP-12 at a MOI of 3. After virus absorption at 37 °C for 1 h, cells were washed three times with phosphate buffered saline (PBS) and fresh medium was added to the wells.

2.2. Intracellular RNA extraction from virus-infected cells

Virus-infected cells were lysed at indicated time points by directly adding 1 ml of Trizol reagent (Invitrogen) to the wells. Total RNA was extracted according to the manufacturer's instructions and re-suspended in 30 µl RNase-free water. The concentration of total RNA was determined by the use of spectrophotometry and adjusted to 100 ng/µl for cDNA synthesis.

2.3. Plasmid construction

Plasmids containing the T7 promoter sequence with MP-12 genomic RNA segments pProT7-L(-), pProT7-M(-), pProT7-S(-) and antigenomic

RNA segments pProT7-L(+), pProT7-M(+), pProT7-S(+) were reported previously (Ikegami et al., 2006). For the generation of a plasmid expressing L mRNA, we used the pProT7-L (+) plasmid as the PCR DNA template. We produced a PCR product by using a forward primer containing Spe I site (5'-TCGAAAACTAGTAGCCCGCCAGGAAG-3'), and a reverse primer containing the end of the transcription termination signal of L RNA (Ikegami et al., 2007) with the Not I site (5'-TCGAATGCGGCCGCGTAGCACTATGCTAGTATC-3'). The purified PCR product replaced a 2.7-kb-long Spe I-Not I region, which contains a portion of the L segment ORF and the entire 3'-NCR, of pProT7-L (+), resulting in the pProT7-L-mRNA like plasmid. The pProT7-M-mRNA like plasmid was similarly generated using a 1.2-kb-long Xba I-Not I region, which contains a portion of the M segment ORF and the entire 3'-NCR, of pProT7-M (+), that was replaced by a purified PCR product. This PCR product was obtained by using a forward primer containing Xba I (5'-CTAGTCTCTAGAGATCACAGACTTTGATGGC-3') and a reverse primer containing the end of the transcription termination signal for M segment (Ikegami et al., 2007) along with the Not I site (5'-TCGAATGCGGCCGCCACCCCAAATTACAAC-3') and the use of the pProT7-M(+) plasmid as a PCR DNA template. Sequence analysis confirmed that both plasmids had the expected sequences and lacked viral sequences after the transcription termination sites.

2.4. In-vitro RNA synthesis

Plasmids were linearized by Not I digestion and subjected to *in-vitro* transcription reactions at 37 °C for 4 h by using the MEGAscript T7 transcription kit (Applied Biosystems/Invitrogen). The samples were then incubated with 2 units of Turbo DNase for 15 min at 37 °C, and RNA was extracted using phenol/chloroform and precipitated using ethanol. To ensure complete removal of residual DNAs, the samples were subjected to a second round of DNase treatment and RNA purification using RNeasy Mini Protocol for RNA Cleanup and On-Column DNase digestion (Qiagen). The on-column DNase treatment was extended to 30 min at room temperature. The concentrations of purified RNA transcripts were determined by using spectrophotometry and quality of RNAs were examined by agarose gel electrophoresis. The molecular copies of synthetic RNAs were calculated from the total molecular weight and length of each RNA segment. At 1 ng of RNA, the copy numbers of full-length L, M, and S segment were 2.925×10^8 copies, 4.820×10^8 copies, and 1.108×10^9 copies respectively. The stocks of *in-vitro* synthesized viral RNAs were subsequently serially diluted to form standard curves used for our RT-qPCR studies.

2.5. Reverse transcription

cDNA synthesis of viral RNAs by using unmodified RT primers (Supplementary Table S1) was performed by using the Superscript-III first strand synthesis system (Invitrogen). Briefly, 100 ng of *in-vitro* synthesized RNA was mixed with 2 μM of strand-specific RT primer. The mixture was incubated at 65 °C for 5 min and then cooled to 4 °C. After addition of the reaction buffer and enzyme mixture, cDNA synthesis was carried out by incubating the sample at 50 °C for 50 min, terminated by heating at 85 °C for 5 min, cooled to 4 °C, and then treated with RNase H at 37 °C for 20 min. RT of viral RNA by using tagged RT primers (Supplementary Table S3) was carried out in a similar method, except that 10 pg of *in-vitro* synthesized RNA or 100 ng of total RNA from virus-infected cells were used as the source of RNA samples. cDNA synthesis was performed by incubating the samples at 55 °C, instead of 50 °C, for 50 min. We used 500 ng of total RNA from virus-infected cells to detect antigenomic RNA segments at the 2 h timepoint because RNA levels were lower than the detection limit early in infection with 100 ng total RNA. Accordingly, the resulting copy numbers for the antigenomic RNA segments were adjusted by dividing by a factor of 5 and plotted with the data obtained for the other timepoints using 100 ng total RNA. The cDNAs were purified using an on-column PCR purification kit (Qiagen). To test for cDNA synthesis caused by RNA self-priming, RT reactions were carried out in the absence of an RT primer.

2.6. Standard PCR

PCRs were performed by using the SsoAdvanced™ Universal SYBR® Green Supermix (Bio Rad). For PCR of cDNAs generated by using unmodified RT primers or no RT primers, 2 μl of cDNA was added to the PCR master mix containing the viral strand-specific PCR primers (Supplementary Table S2). For cDNAs generated by tagged RT primers and purified by on-column purification, 1 μl of cDNA was added to the PCR master mix containing the non-viral tagged sequence as a forward primer and a viral strand-specific PCR reverse primer (Supplementary Table S4). For both PCRs, thermocycling conditions were as follows: 95 °C for 30 s, 35 cycles of 95 °C for 15 s and 60 °C for 20 s. PCR products were analyzed by gel electrophoresis. Gel Images are scanned, cropped, and assembled by AlphaEase FC Software.

2.7. Quantitative PCR

The real time qPCR assays were prepared using the SsoAdvanced™ Universal SYBR® Green Supermix. Total RNAs from virus-infected cells were subjected to RT using tagged strand-specific RT primers as stated before. After cDNA purification, 1 μl of cDNA was added to the PCR master mix containing the non-viral tagged sequence as a forward primer and a viral strand-specific PCR reverse primer (Supplementary Table S4). Thermocycling conditions were the same as standard PCR, followed by melting curve analysis. The assays were performed by the CFX96 Touch Real-time PCR detection system and analyzed using the provided software (BioRad CFX Manager 3.1).

3. Results

3.1. Strand-specific RT-PCR assay design using unmodified primers fails to selectively amplify target viral RNA segments

Our initial approach for quantifying RVFV genomic and antigenomic segments was to synthesize cDNAs by using RT primers, each of which specifically bind to the 3' NCR of each viral RNA segment (Fig. 1), and subsequent amplification of the cDNA products by PCR. Antigenomic L segment and M segment have the same orientation as L mRNA and M mRNA, respectively (Fig. 1). As transcription of both mRNAs is terminated at the transcription termination site(Ikegami et al., 2007; Lara et al., 2011) located within the 3' NCR of these antigenomic segments, both mRNAs lack sequences present downstream of the transcription termination sites. To determine the abundances of antigenomic L and M segments, we designed RT primers that bind downstream of their transcription termination sites such that the RT primers would not bind to L and M mRNAs and only amplify full-length antigenomic segments. Genomic S segment and antigenomic S segment serve as templates for N mRNA and NSs mRNA, respectively (Fig. 1). As RT primers used for the cDNA synthesis of genomic S segment and antigenomic S segment had the same sequence as N mRNA and NSs mRNA, respectively, they would not bind to these mRNAs. Supplementary Table S1 lists the RT primers used for each viral segment. Our initial experimental design used the PCR primer sets reported by others (Maquart et al., 2014; Naslund et al., 2008; Wilson et al., 2013) (Supplementary Table S2).

To test whether this experimental design worked, we generated full-length genomic and antigenomic viral RNAs for each segment by using *in-vitro* transcription. After DNase treatment of the samples, these RNAs were subjected to cDNA synthesis by using RT primers, each of which binds to genomic L, M and S segment, and subsequent PCR amplification by using the PCR primer sets reported by others(Maquart et al., 2014; Naslund et al., 2008; Wilson et al., 2013). Surprisingly, we

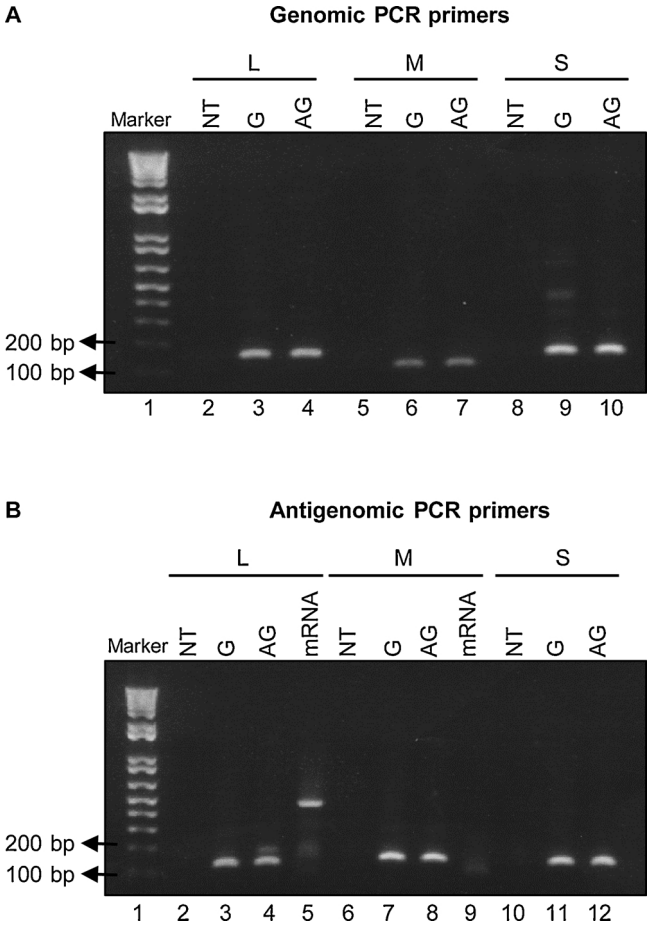

Fig. 2. Standard RT-PCR using unmodified primers does not display strand-specificity. (A) 100 ng of *in-vitro* synthesized RNAs corresponding to the genomic (G) and antigenomic (AG) segments of L, M, and S RNAs were used for cDNA synthesis using unmodified RT primers specific for genomic L, M, and S segments respectively. The corresponding cDNAs were subjected to PCR by using unmodified PCR primer sets, specific for genomic L (lanes 2–4), M (lanes 5–7) and S (lanes 8–10) segments. NT represents the "no template" control for RT-PCR analysis (lanes 2, 5 and 8). (B) 100 ng of *in-vitro* synthesized RNAs corresponding to the genomic (G), antigenomic (AG) segments of L, M, and S RNAs, and cognate mRNAs (mRNA) of L and M segments were used for cDNA synthesis using unmodified RT primers specific for antigenomic L, M, and S segments respectively. The corresponding cDNAs were subjected to PCR by using an unmodified PCR primer set, specific for antigenomic L (lanes 2–5), M (lanes 6–9) and S (lanes 10–12) segments. Lane 1 in.(A) and (B) represents the DNA size marker, and the location of the markers having 100 and 200 base pairs (bp) bands are indicated by arrows. The PCR products were analyzed by agarose gel electrophoresis. NT represents the no template control for RT-PCR analysis (lanes 2, 6 and 10).

detected PCR products of the expected sizes from target genomic segments, whereas we also detected PCR products of the same sizes from corresponding antigenomic segments (Fig. 2A). We performed similar experiments, in which *in-vitro* synthesized genomic L, M and S segment, antigenomic L, M and S segment, and L and M mRNAs, were subjected to cDNA synthesis by using RT primers, each of which designed to bind to each full-length antigenomic segment. Amplification of the cDNAs by using the reported PCR primers resulted in generation of the PCR products of the expected sizes from both antigenomic and genomic segment RNAs and an unexpected PCR product of ~500 bp from L mRNA (Fig. 2B). These data showed that this experimental design was unable to selectively amplify target RNAs. To exclude the possibility of incomplete DNA digestion after *in-vitro* transcription leading to the generation of the PCR products from low levels of residual DNAs, the RNA samples were directly subjected to the PCR reaction. No PCR products were generated (Supplementary Fig. S1), demonstrating absence of DNA contamination in the RNA samples.

3.2. Primer-independent cDNA synthesis prevents selective amplification of target viral RNAs

Multiple studies have reported a phenomenon known as self-primed reverse transcription, where cDNA can be generated in the absence of an RT primer(Beiter et al., 2007; Craggs et al., 2001; Feng et al., 2012; Haist et al., 2015; Lanford and Chavez, 1999; Lim et al., 2013; Peyrefitte et al., 2003; Plaskon et al., 2009; Tuiskunen et al., 2010; Vashist et al., 2012). The self-priming in the absence of the RT primer is most probably due to the intrinsic ability of the RNA itself or the presence of small RNA fragments in RNA preparations that can serve as primers. To test whether self-primed reverse transcription occurred in this assay system, we performed cDNA synthesis from synthetic genomic and antigenomic viral segments along with RNAs isolated from RVFV-infected cells in the absence of RT primers. The samples were then subjected to PCR. In all samples, we detected PCR products of the same sizes as those generated by amplification of the correct cDNAs by using PCR primer sets (Fig. 3), suggesting that cDNA was synthesized in the absence of the RT primer from these viral RNAs. Therefore, we concluded that cDNAs produced by false-priming, possibly due to RNA self-priming, underwent PCR-mediated amplification, preventing strand-specificity of the assay system.

3.3. Strand-specific RT-PCR using 'tagged' RT primers selectively amplifies the target viral RNA segment

To establish a strand-specific RT-qPCR assay, we modified our assay by increasing the annealing temperature during reverse transcription from 50 °C to 55 °C and by using 'tagged' RT primers (Supplementary Table S3). Increasing the annealing temperature in the reverse transcription step has been shown to reduce non-specific primer binding (Feng et al., 2012; Lanford and Chavez, 1999; Lim et al., 2013). The tagged primer method has been used in numerous studies to overcome false-priming issues(Bannister et al., 2010; Brennan et al., 2014; Chatterjee et al., 2012; Kawakami et al., 2011; Lim et al., 2013; Peyrefitte et al., 2003; Plaskon et al., 2009; Strydom and Pietersen, 2018; Tuiskunen et al., 2010; Vashist et al., 2012). In this modified assay, cDNA synthesis was performed by using a tagged RT primer complementary to each of the target RNA segments (Fig. 4). Each tagged RT primer had a non-viral tag sequence, modified from Brennan et al., (Brennan et al., 2014) at the 5'-end. Hence, cDNAs that are synthesized by using the tagged RT primer, but not those synthesized by false-priming, carry the 'tag' sequence at the 5'-end. The tagged RT primer for the antigenomic M segment and that for the antigenomic L segment were designed not to bind to M mRNA and L mRNA, respectively. The tag sequence of the RT primer was used as the forward primer (5'-GGCCGTCATGGTGGCGAATA-3') and a strand-specific primer was used as the reverse primer in PCR. Use of the tag sequence as the forward primer ensures that only primer-driven tagged cDNA, but not those generated by false-priming, gets amplified during PCR.

To determine whether a combination of forward tag PCR primer and strand-specific reverse PCR primer amplifies cDNAs synthesized by false-priming, we performed cDNA synthesis from *in-vitro* synthesized genomic and antigenomic viral segments and RNAs from RVFV-infected cells in the absence of the RT primers. The samples were then subjected to PCR amplification by using a forward tag PCR primer and strand-specific reverse PCR primer for each of the genomic and antigenomic viral segments (Supplementary Table S4). No PCR products were generated (Supplementary Fig. S2A and S2B), demonstrating that a combination of the forward tag PCR primer and the strand-specific reverse PCR primer did not amplify cDNAs produced by false-priming.

We next tested whether use of the tagged RT primer for cDNA

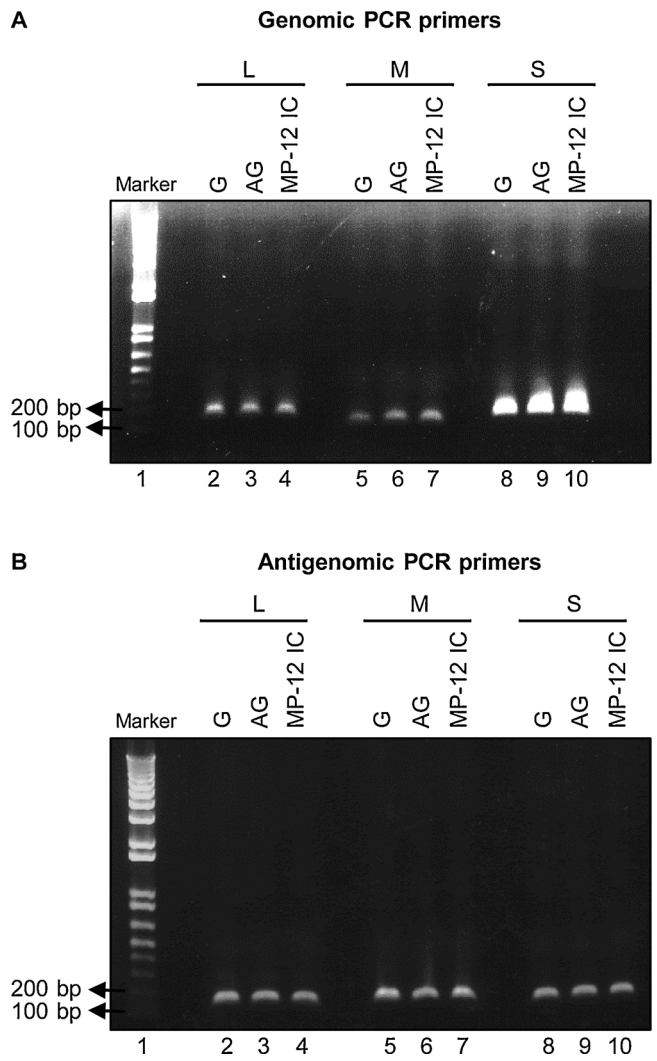

Fig. 3. Primer-independent cDNA synthesis of viral RNA impairs standard RT-PCR strand-specificity. 100 ng of *in-vitro* synthesized RNAs corresponding to the genomic (G) and antigenomic (AG) segments of L, M, and S RNAs and intracellular RNAs from RVFV-infected cells (MP-12 IC) were used for cDNA synthesis without the use of specific RT primers. (A) After cDNA synthesis, the samples underwent PCR using unmodified PCR primer sets, specific for genomic L (lanes 2–4), M (lanes 5–7), and S (lanes 8–10) segments. (B) Experiments were done similar to (A), except that the samples underwent PCR using unmodified PCR primer sets, specific for antigenomic L (lanes 2–4), M (lanes 5–7), and S (lanes 8–10) segments. Lane 1 in.(A) and (B) represents the DNA size marker, and the location of the markers having 100 and 200 base pairs (bp) bands are indicated by arrows. The PCR products were analyzed by agarose gel electrophoresis.

synthesis and subsequent PCR using forward tag PCR primer and strand-specific reverse PCR primer sets lead to selective amplification of the target RNA. We used *in-vitro* synthesized genomic and antigenomic L, M and S segments and L and M mRNAs as source RNAs. As residual RT primer present during PCR amplification can also cause false-priming (Craggs et al., 2001; Feng et al., 2012; Lim et al., 2013; Peyrefitte et al., 2003; Vashist et al., 2012), we purified the cDNAs after reverse transcription to remove residual tagged RT primers and reverse transcriptase, and then subjected them to PCR amplification using the forward tag PCR primer and strand-specific reverse PCR primer for each target RNA (Supplementary Table S4). We detected PCR products of the expected sizes only from the target RNA templates (Fig. 5), demonstrating selective amplification of the target RNAs.

3.4. Establishment of strand-specific RT-qPCR assays for genomic and antigenomic RVFV RNAs

As the experimental approach described above successfully amplified the target viral RNAs, we proceeded to further validate and establish the RT-qPCR assay and examined its sensitivity and selectivity. To determine absolute copy number for target viral RNAs that are detectable in this assay, we performed an RT-qPCR assay by using known copy numbers of *in-vitro* transcribed RNA and established standard curves for each viral segment, where 10^3 to 10^{10} copies of genomic and antigenomic L and M segments and 10^4 to 10^{11} copies of genomic and antigenomic S segments showed strong linearity with 0.992 or better correlation coefficient (R^2) values (Fig. 6 and Table 1).

We next tested whether this assay was capable of quantifying target viral RNAs in the presence of RNAs in the opposite sense. We prepared RNA samples, where 10^4 - 10^8 copies of target genomic or antigenomic L or M segments were mixed with 10^6 copies of their opposite-strand RNA and 10^5 - 10^9 copies of target genomic or antigenomic S segment were mixed with 10^7 copies of their opposite-strand RNA, and used them as RNA sources for cDNA synthesis. After cDNA synthesis using specific tagged RT primers for the target RNA, we purified cDNAs and performed qPCR. The amounts of all target RNAs were accurately determined under this experimental condition, demonstrating that this strand-specific RT-qPCR assay was able to measure the amounts of the target RNAs in the presence of up to ˜100-fold excess amounts of their opposite-strand RNAs (Fig. 7). Taken together, these data demonstrate that the modified strand-specific RT-qPCR assay was effective for overcoming false priming and allowed us to distinguish between all of the genomic and antigenomic RVFV RNAs.

3.5. Kinetics of viral RNA accumulation in RVFV-infected cells

We used this newly established strand-specific RT-qPCR assay to investigate the intracellular accumulation kinetics of RVFV RNAs following infection in Vero E6 cells and Huh7 cells, a hepato-cellular carcinoma cell line (Nakabayashi et al., 1982), at a multiplicity of infection (MOI) of 3. We determined the amounts of intracellular genomic and antigenomic L, M and S segments at 2, 4, 6, 8, 12, 16, and 20 h post-infection (p.i.) (Fig. 8).

In both cell lines, accumulation of all three genomic RNA segments were substantially higher than their antigenomic counterparts throughout the course of infection, with the exception of M segment at 6–8 h p.i., in Vero E6 cells and 4–12 h p.i. in Huh7 cells, showing similar levels of accumulation for genomic and antigenomic RNAs. Accumulation of antigenomic M segment in both cell lines were higher relative to antigenomic L and S segment after 4 h p.i., being more prominent in Huh7 cells (Supplementary Fig. S3B). We also noted that early in infection (4–6 h p.i.), genomic S segment copy numbers were higher compared to genomic L and M segments (Fig. 8 and Supplementary Fig. S3A).

4. Discussion

The present study reported the development of a RT-qPCR assay that determines the amounts of genomic and antigenomic L, M and S segments of RVFV; this assay represents the first system that can distinguish and measure the accumulation of all genomic and antigenomic viral RNA segments in any bunyaviruses. Several methods have been used to detect and quantify the different viral RNA species generated during RVFV infection, including radiolabeling, Northern blot, *in-situ* hybridization, and RT-qPCR assays (Brennan et al., 2014; Garcia et al., 2001; Gauliard et al., 2006; Ikegami et al., 2005; Maquart et al., 2014; Naslund et al., 2008; Wichgers Schreur and Kortekaas, 2016; Wilson et al., 2013). Limitations of these studies include limited sensitivity, different probe efficiencies, and the inability to distinguish antigenomic RNA from mRNA and genomic RNA from antigenomic RNA. Multiple

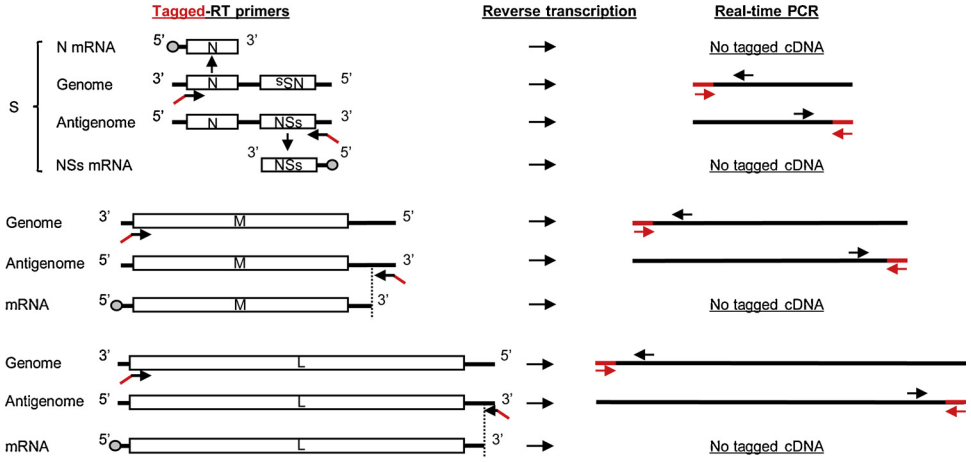

Fig. 4. Schematic diagram of modified RT-qPCR with tagged RT primers and modified PCR primer sets. Left panel shows schematic diagram of RVFV RNAs and binding sites of tagged RT primers to viral RNA segments. cDNA synthesis is performed using a tagged RT primer complementary to either genomic or antigenomic viral RNA segments. The tagged non-viral sequence, shown in red, is attached to the 5'-end of each strand-specific RT primer. For genomic segments, the tagged genomic RT primers bind to the 3'-end of these RNAs. Note that the tagged genomic RT primer binds to the 3'-end of genomic S segment, but not N mRNA, as the RT primer is in the same orientation as N mRNA. The same principle is applied for the tagged RT primer for antigenomic S segment, which does not bind to NSs mRNA. The tagged RT primers for antigenomic M and L segments bind downstream of the transcription termination sites of these segments. The dashed lines indicate the 3'-ends of L and M mRNAs compared to the full-length antigenomic segments. The right panel outlines the PCR of the cDNA products by using the forward PCR primer (red arrows), which is the tag portion of the RT primer, and a strand-specific reverse PCR primer (black arrows). Use of the tagged portion as a forward PCR primer ensures that only primer-driven tagged cDNAs undergo amplification.

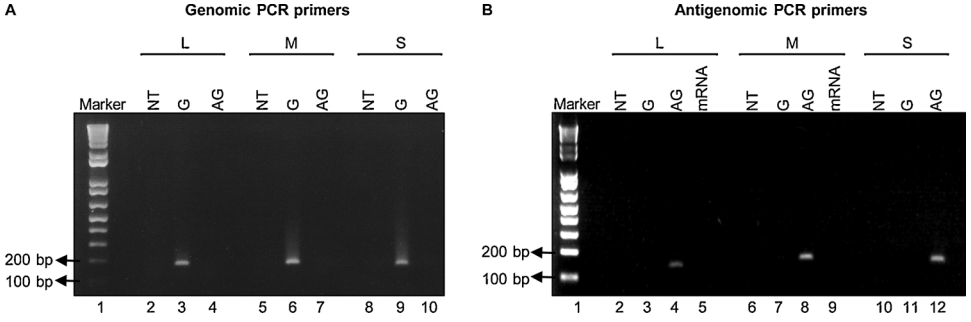

Fig. 5. Validation of a strand-specific RT-qPCR using modified tagged RT primers and PCR primer sets. (A) 10 pg of *in-vitro* synthesized RNAs corresponding to the genomic (G) and antigenomic (AG) segments of L, M, and S RNAs were used for cDNA synthesis using tagged RT primers specific for genomic L, M, and S segments. The corresponding cDNAs were subjected to PCR by using PCR primer sets with the 'tag' sequence as the forward primer and a segment-specific reverse primer that selectively amplifies genomic L (lanes 2–4), M (lanes 5–7) and S (lanes 8–10) segments. NT represents the "no template" control for RT-PCR analysis (lanes 2, 5 and 8). (B) 10 pg of *in-vitro* synthesized RNAs corresponding to the genomic (G), antigenomic (AG) segments of L, M, and S RNAs, and cognate mRNAs (mRNA) of L and M segments were used for cDNA synthesis by using tagged RT primers specific for antigenomic L, M, and S segments. The corresponding cDNAs were subjected to PCR using PCR primer sets with the 'tag' sequence as the forward primer and a segment-specific reverse primer that selectively amplifies antigenomic L (lanes 2–5), M (lanes 6–9) and S (lanes 10–12) segments. NT represents the "no template" control for RT-PCR analysis (lanes 2, 6 and 10). Lane 1 in.(A) and (B) represents the DNA size marker, and the location of the markers having 100 and 200 base pairs (bp) bands are indicated by arrows. The PCR products were analyzed by agarose gel electrophoresis.

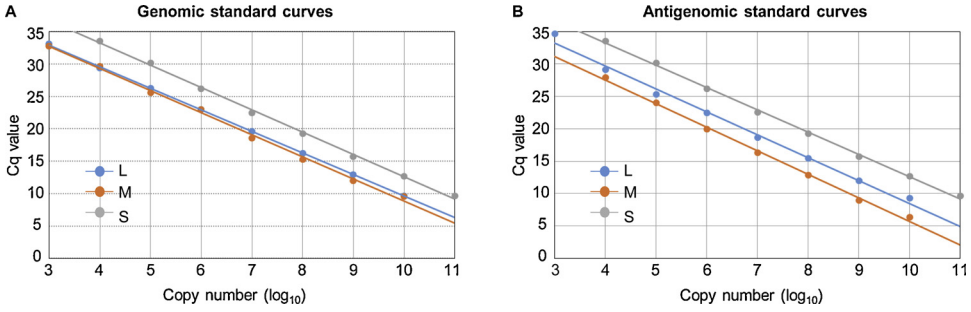

Fig. 6. Standard curves for genomic and antigenomic segments. Standard curves for (A) genomic and (B) antigenomic viral segments were generated by plotting the quantification cycle (Cq) value against the input of *in-vitro* transcribed RNA of known copy numbers. *In-vitro* synthesized genomic RNA segments (A) and antigenomic RNA segments (B) were serially diluted ten-fold, (10^{10} to 10^3 copies) for L (blue) and M (orange) segments and (10^{11} to 10^4 copies) for S segment (grey) and were used to generate standard curves.

groups have reported the use of RT-qPCR approaches to quantitate RVFV RNA load, however these assays were not designed to specifically target individual replicative RNA species(Garcia et al., 2001; Maquart et al., 2014; Naslund et al., 2008; Wilson et al., 2013). Additionally, these assays do not take into account cDNA synthesized due to false priming.

The assay developed in this study incorporated the combined use of the tagged RT primer and the forward tag and the strand-specific reverse PCR primers, which eliminated amplification of cDNAs generated by false-priming (Fig. 5). This modified assay excluded amplification of viral mRNAs (Fig. 5B) and accurately measured between 10^3 to 10^{10} copies of the genomic and antigenomic L and M segments and between 10^4 to 10^{11} copies of the genomic and antigenomic S segments in samples (Fig. 6). The assay was also able to accurately determine the amounts of target viral RNAs present in up to ~100-fold excess amounts of their opposite-strand RNAs (Fig. 7). Brennan et al., reported a similar RT-qPCR assay, where tagged RT primer and sets of forward tag and strand-specific reverse PCR primers were used to determine the amounts of the genomic and antigenomic RVFV M and S segments, however their assay did not include the measuring method for the genomic and antigenomic L segments (Brennan et al., 2014). Our RT-qPCR assay design benefited from their study; we used the same tag sequence used in their tagged RT primers, except that our tag sequence had an extra 'A' at the 3'-end, and used the same strand-specific reverse

Table 1
Validation parameters for RT-qPCR.

Genome	Sensitivity (Copies)	Linear Regression			
		Slope	*Intercept*	*Amplification efficiency (%)*	R^2 *value*
L segment	10^3	−3.329	44.471	99.7	0.998
M segment	10^3	−3.408	45.288	96.5	0.996
S segment	10^4	−3.446	47.207	95.1	0.998
Antigenome					
L segment	10^3	−3.535	45.480	91.8	0.992
M segment	10^4	−3.645	44.609	88.1	0.997
S segment	10^4	−3.222	44.611	104.3	0.995

PCR primer for the genomic-sense S RNA. Because the transcription termination signal for L mRNA is located very close to the 3'-end of the antigenomic L RNA(Ikegami et al., 2007; Lara et al., 2011), it was necessary to determine an appropriate binding site of the tagged RT primer for cDNA synthesis of antigenomic L segment, but not for cDNA synthesis of L mRNA, within ˜20 nt from the 3'-end of antigenomic L segment. After testing several tagged RT primer candidates, we were able to identify an appropriate tagged RT primer for antigenomic L segment.

Like other past studies that have reported self-primed reverse transcription in various viruses (Beiter et al., 2007; Craggs et al., 2001; Feng et al., 2012; Haist et al., 2015; Lanford and Chavez, 1999; Lim et al., 2013; Peyrefitte et al., 2003; Plaskon et al., 2009; Tuiskunen et al., 2010; Vashist et al., 2012), our data suggested synthesis of cDNAs in the absence of an RT primer from *in-vitro* synthesized RVFV RNAs as

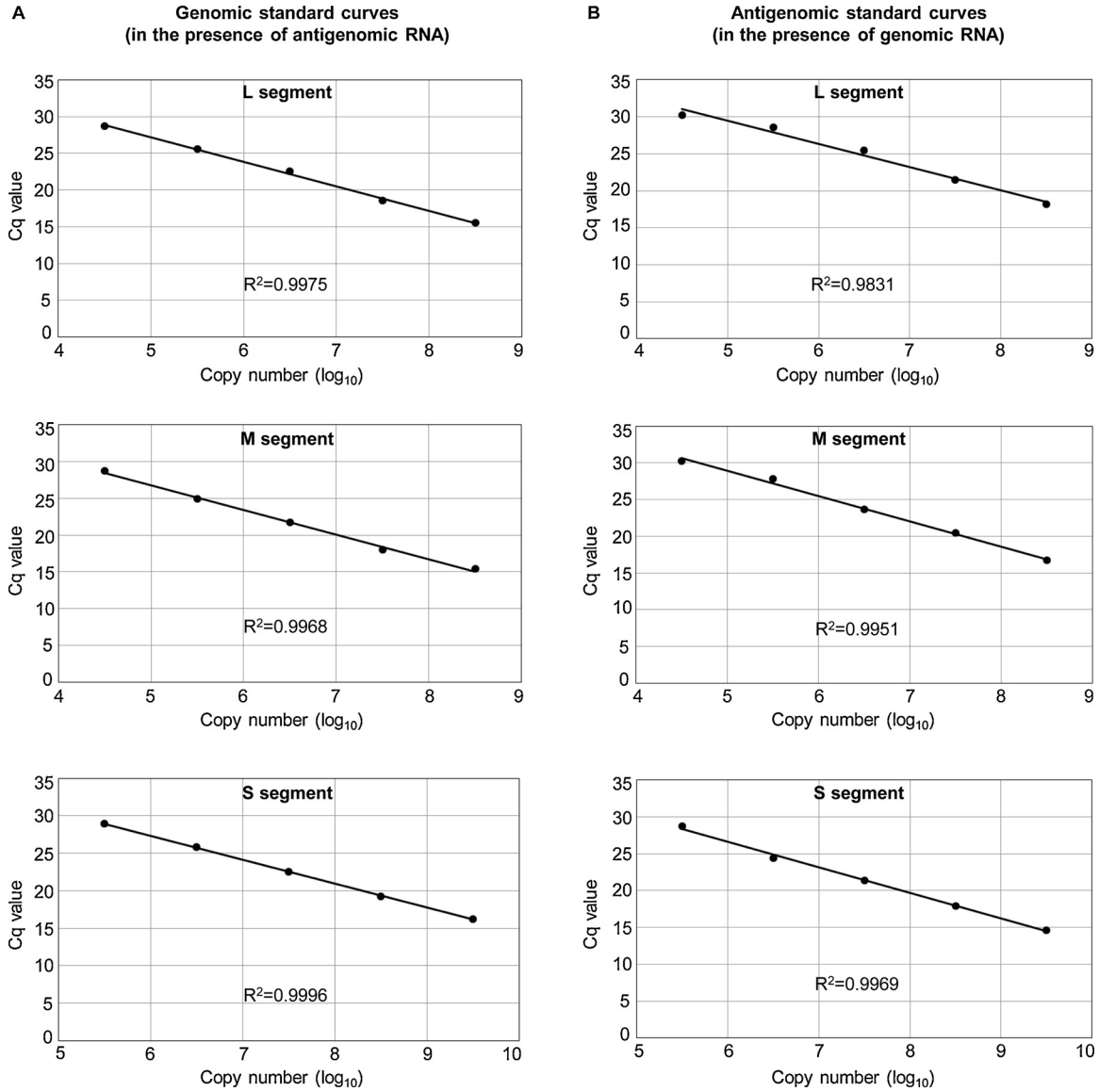

Fig. 7. Demonstration of strand-specific RT-qPCR in the presence of opposite-sense RNA transcripts. (A) Genomic standard curves were generated by synthesizing cDNAs from indicated copy number of *in-vitro* transcribed genomic L (top panel), M (middle panel), and S (bottom panel) segments by using a tagged RT primer in the presence of 10^6 copies of antigenomic L, 10^6 copies of antigenomic M and 10^7 copies of antigenomic S segments, respectively. The cDNAs were subjected to PCR by using primer sets with the tag sequence as the forward primer and a specific reverse PCR primer designed specifically for amplifying genomic L, M and S segments. (B). Antigenomic standard curves were generated by synthesizing cDNAs from the indicated copy numbers of *in-vitro* transcribed antigenomic L (top panel), M (middle panel), and S (bottom panel) segments using a tagged RT primer in the presence of 10^6 copies of genomic L, 10^6 copies of genomic M and 10^7 copies of genomic S segments, respectively. The cDNAs were subjected to PCR using primer sets with the tag sequence as the forward primer and a specific reverse PCR primer designed specifically for amplifying antigenomic L, M and S segments. The linear regression (R^2) value is displayed on each graph.

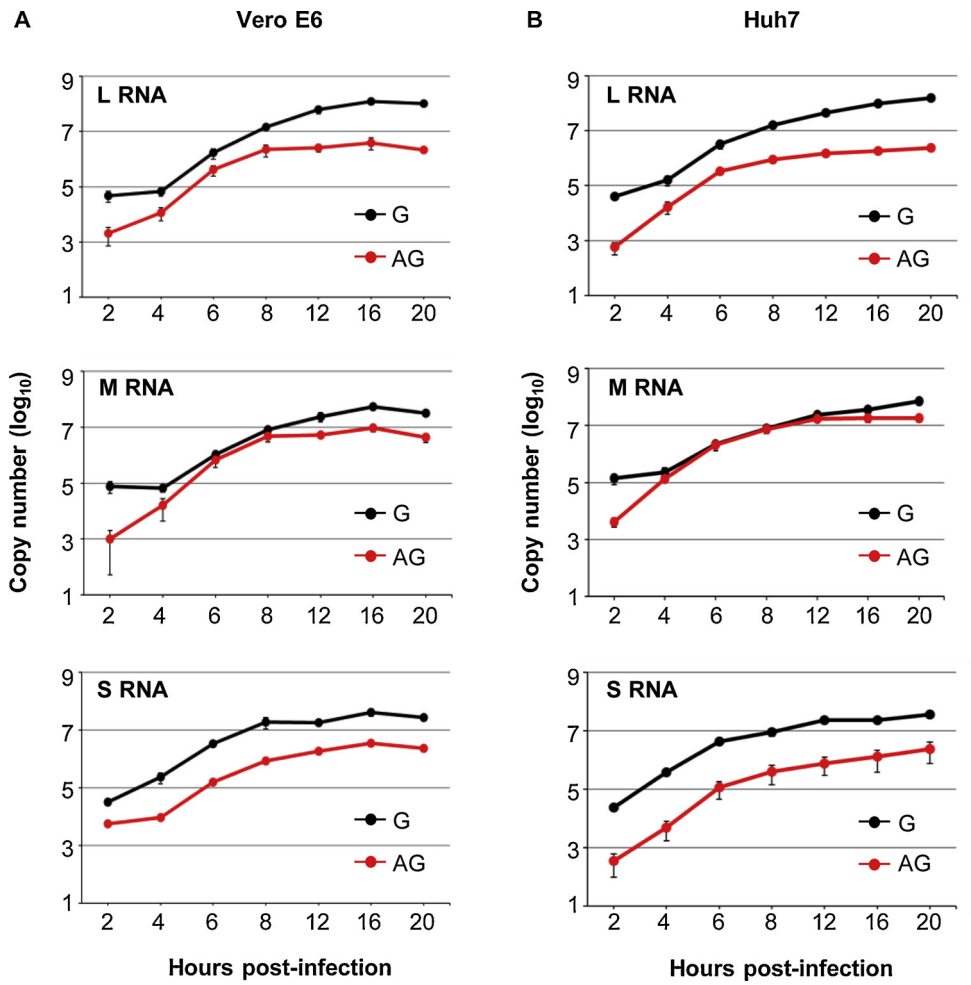

Fig. 8. Accumulation kinetics of genomic and antigenomic viral RNA segments in RVFV-infected cells. (A) Vero E6 and (B) Huh7 cells were infected with RVFV at an MOI of 3. Total intracellular RNAs were extracted in triplicate at the indicated times p.i. Total RNAs were subjected to strand-specific RT-qPCR and the copy numbers for each viral segment, which were determined with synthetic viral RNA as a reference standard, are plotted. Error bars represent the mean (+/− the standard deviation) of triplicate experiments.

well as intracellular RNAs obtained from RVFV-infected cells (Fig. 3). Because the 5'- and 3'-ends of both genomic and antigenomic RVFV RNA segments have a stretch of short complementary sequences that form a double-stranded panhandle structure(Gaudreault et al., 2019; Hornak et al., 2016; Ikegami, 2012; Sun et al., 2018), a likely mechanism of primer-independent cDNA synthesis in RVFV RNAs is that reverse transcriptase recognizes the panhandle structure and initiates cDNA synthesis.

By using our newly developed RT-qPCR assay, we examined the accumulation kinetics of replicating RVFV RNAs in Vero E6 and Huh7 cells (Fig. 8); the former is widely used for studies of RVFV replication and preparation of virus stocks (Ikegami et al., 2006) and the latter, a hepato-cellular carcinoma cell line (Nakabayashi et al., 1982), was selected because one of the major target organs of RVFV in mammals is the liver (Gommet et al., 2011; Terasaki and Makino, 2015). To our knowledge, this is the first study demonstrating the accumulation kinetics of replicating viral RNA species in bunyavirus-infected cells. We noted similar accumulation kinetics of viral RNAs in both cell lines. The amounts of the genomic RNA segments were always higher than corresponding antigenomic RNA segments throughout the infection, except that the amounts of genomic and antigenomic M segments were similar at 6–8 h p.i. in Vero cells and at 4–12 h p.i. in Huh7 cells. Our finding of similar levels of the genomic and antigenomic M segments in RVFV-infected cells are a marked contrast to accumulation of viral RNAs in cells infected with positive-stranded RNAs, where abundances of genomic RNAs always exceed antigenomic RNAs. Currently, it is unclear why only M segment showed similar accumulations of genomic and antigenomic RNAs at certain times p.i.

In both cell lines, genomic S RNA, but not genomic L and M RNAs, rapidly accumulated from 2 to 4 h p.i. (Fig. 8 and Supplementary Fig. S3A). Antigenomic S RNA is packaged efficiently into RVFV particles, and we previously reported that the incoming antigenomic S RNA serves as template for the synthesis of NSs mRNA immediately following RVFV infection, leading to NSs expression early in infection (Ikegami et al., 2005). Expression of NSs immediately after infection would be critical for efficient virus replication in mammalian hosts, as the incoming RVFV RNPs trigger RIG-I-mediated antiviral innate immune signaling(Bouloy et al., 2001; Ly and Ikegami, 2016; Terasaki and Makino, 2015). Rapid accumulation of genomic S segment from 2 to 4 h p.i. suggest that the incoming antigenomic S segment also serves as the template for genomic S RNA replication. This results in efficient genomic S RNA accumulation, which was higher than the accumulation of genomic L and M segments from 4 to 6 h p.i. (Supplementary Fig. 3A). Efficient accumulation of genomic S RNA, which serves as the template for N mRNA, during the early phase of infection may lead to efficient accumulation of N protein early in infection resulting in optimal virus replication.

In conclusion, our strand-specific RT-qPCR assay determined the amounts of genomic and antigenomic RVFV RNAs with accuracy and specificity, allowing us to determine the accumulation kinetics of these

viral RNAs in infected cells. Overall, our assay system will be a valuable tool to examine the replication mechanisms of RVFV.

The author(s) declare no competing interests.

Declaration of Competing Interest

The author(s) declare no competing interests.

Acknowledgements

This work was supported by Public Health Service grants, AI114657, AI114657-S1, AI117445, AI27984 from the NIH and the IHII pilot grant from the University of Texas Medical Branch.

Appendix A. Supplementary data

Supplementary material related to this article can be found, in the online version, at doi:https://doi.org/10.1016/j.jviromet.2019.113701.

References

Al-Hazmi, A., Al-Rajhi, A.A., Abboud, E.B., Ayoola, E.A., Al-Hazmi, M., Saadi, R., Ahmed, N., 2005. Ocular complications of Rift Valley fever outbreak in Saudi Arabia. Ophthalmology 112, 313–318.

Albarino, C.G., Bird, B.H., Nichol, S.T., 2007. A shared transcription termination signal on negative and ambisense RNA genome segments of Rift Valley fever, sandfly fever Sicilian, and Toscana viruses. J. Virol. 81, 5246–5256.

Alrajhi, A.A., Al-Semari, A., Al-Watban, J., 2004. Rift Valley fever encephalitis. Emerg. Infect. Dis. 10, 554–555.

Balkhy, H.H., Memish, Z.A., 2003. Rift Valley fever: an uninvited zoonosis in the Arabian peninsula. Int. J. Antimicrob. Agents 21, 153–157.

Bannister, R., Rodrigues, D., Murray, E.J., Laxton, C., Westby, M., Bright, H., 2010. Use of a highly sensitive strand-specific quantitative PCR to identify abortive replication in the mouse model of respiratory syncytial virus disease. Virol. J. 7.

Beiter, T., Reich, E., Weigert, C., Niess, A.M., Simon, P., 2007. Sense or antisense? False priming reverse transcription controls are required for determining sequence orientation by reverse transcription-PCR. Anal. Biochem. 369, 258–261.

Bouloy, M., Janzen, C., Vialat, P., Khun, H., Pavlovic, J., Huerre, M., Haller, O., 2001. Genetic evidence for an interferon-antagonistic function of Rift Valley fever virus nonstructural protein NSs. J. Virol. 75, 1371–1377.

Bouloy, M., Weber, F., 2010. Molecular biology of rift valley fever virus. Open Virol. J. 4, 8–14.

Brennan, B., Welch, S.R., Elliott, R.M., 2014. The consequences of reconfiguring the ambisense S genome segment of Rift Valley fever virus on viral replication in mammalian and mosquito cells and for genome packaging. PLoS Pathog. 10 e1003922.

Chatterjee, S.N., Devhare, P.B., Lole, K.S., 2012. Detection of negative-sense RNA in packaged hepatitis E virions by use of an improved strand-specific reverse transcription-PCR method. J. Clin. Microbiol. 50, 1467–1470.

Craggs, J.K., Ball, J.K., Thomson, B.J., Irving, W.L., Grabowska, A.M., 2001. Development of a strand-specific RT-PCR based assay to detect the replicative form of hepatitis C virus RNA. J. Virol. Methods 94, 111–120.

Deutman, A.F., Klomp, H.J., 1981. Rift Valley fever retinitis. Am. J. Ophthalmol. 92, 38–42.

Feng, L., Lintula, S., Ho, T.H., Anastasina, M., Paju, A., Haglund, C., Stenman, U.H., Hotakainen, K., Orpana, A., Kainov, D., Stenman, J., 2012. Technique for strand-specific gene-expression analysis and monitoring of primer-independent cDNA synthesis in reverse transcription. BioTechniques 52, 263–270.

Garcia, S., Crance, J.M., Billecocq, A., Peinnequin, A., Jouan, A., Bouloy, M., Garin, D., 2001. Quantitative real-time PCR detection of Rift Valley fever virus and its application to evaluation of antiviral compounds. J. Clin. Microbiol. 39, 4456–4461.

Gargan 2nd, T.P., Clark, G.G., Dohm, D.J., Turell, M.J., Bailey, C.L., 1988. Vector potential of selected North American mosquito species for Rift Valley fever virus. Am. J. Trop. Med. Hyg. 38, 440–446.

Gaudreault, N.N., Indran, S.V., Balaraman, V., Wilson, W.C., Richt, J.A., 2019. Molecular aspects of Rift Valley fever virus and the emergence of reassortants. Virus Genes 55, 1–11.

Gauliard, N., Billecocq, A., Flick, R., Bouloy, M., 2006. Rift Valley fever virus noncoding regions of L, M and S segments regulate RNA synthesis. Virology 351, 170–179.

Gommet, C., Billecocq, A., Jouvion, G., Hasan, M., Zaverucha do Valle, T., Guillemot, L., Blanchet, C., van Rooijen, N., Montagutelli, X., Bouloy, M., Panthier, J.J., 2011. Tissue tropism and target cells of NSs-deleted rift valley fever virus in live immunodeficient mice. PLoS Negl. Trop. Dis. 5 e1421.

Haist, K., Ziegler, C., Botten, J., 2015. Strand-specific quantitative reverse transcription-polymerase chain reaction assay for measurement of arenavirus genomic and antigenomic RNAs. PLoS One 10 e0120043.

Hopkins, K., Cherry, S., 2013. Bunyaviral cap-snatching vs. decapping: recycling cell cycle mRNAs. Cell Cycle 12, 3711–3712.

Hornak, K.E., Lanchy, J.M., Lodmell, J.S., 2016. RNA encapsidation and packaging in the phleboviruses. Viruses 8.

House, J.A., Turell, M.J., Mebus, C.A., 1992. Rift Valley fever: present status and risk to the Western Hemisphere. Ann. N. Y. Acad. Sci. 653, 233–242.

Ikegami, T., 2012. Molecular biology and genetic diversity of Rift Valley fever virus. Antiviral Res. 95, 293–310.

Ikegami, T., Makino, S., 2011. The pathogenesis of Rift Valley fever. Viruses 3, 493–519.

Ikegami, T., Won, S., Peters, C.J., Makino, S., 2005. Rift Valley fever virus NSs mRNA is transcribed from an incoming anti-viral-sense S RNA segment. J. Virol. 79, 12106–12111.

Ikegami, T., Won, S., Peters, C.J., Makino, S., 2006. Rescue of infectious Rift Valley fever virus entirely from cDNA, analysis of virus lacking the NSs gene, and expression of a foreign gene. J. Virol. 80, 2933–2940.

Ikegami, T., Won, S., Peters, C.J., Makino, S., 2007. Characterization of Rift Valley fever virus transcriptional terminations. J. Virol. 81, 8421–8438.

Kawakami, E., Watanabe, T., Fujii, K., Goto, H., Watanabe, S., Noda, T., Kawaoka, Y., 2011. Strand-specific real-time RT-PCR for distinguishing influenza vRNA, cRNA, and mRNA. J. Virol. Methods 173, 1–6.

Lanford, R.E., Chavez, D., 1999. Strand-specific rTth RT-PCR for the analysis of HCV replication. Methods Mol. Med. 19, 471–481.

Lara, E., Billecocq, A., Leger, P., Bouloy, M., 2011. Characterization of wild-type and alternate transcription termination signals in the Rift Valley fever virus genome. J. Virol. 85, 12134–12145.

Lim, S.M., Koraka, P., Osterhaus, A.D., Martina, B.E., 2013. Development of a strand-specific real-time qRT-PCR for the accurate detection and quantitation of West Nile virus RNA. J. Virol. Methods 194, 146–153.

Linthicum, K.J., Britch, S.C., Anyamba, A., 2016. Rift Valley fever: an emerging mosquito-borne disease. Annu. Rev. Entomol. 61, 395–415.

Ly, H.J., Ikegami, T., 2016. Rift Valley fever virus NSs protein functions and the similarity to other bunyavirus NSs proteins. Virol. J. 13, 118.

Madani, T.A., Al-Mazrou, Y.Y., Al-Jeffri, M.H., Mishkhas, A.A., Al-Rabeah, A.M., Turkistani, A.M., Al-Sayed, M.O., Abodahish, A.A., Khan, A.S., Ksiazek, T.G., Shobokshi, O., 2003. Rift Valley fever epidemic in Saudi Arabia: epidemiological, clinical, and laboratory characteristics. Clin. Infect. Dis. 37, 1084–1092.

Maquart, M., Temmam, S., Heraud, J.M., Leparc-Goffart, I., Cetre-Sossah, C., Dellagi, K., Cardinale, E., Pascalis, H., 2014. Development of real-time RT-PCR for the detection of low concentrations of Rift Valley fever virus. J. Virol. Methods 195, 92–99.

Murakami, S., Terasaki, K., Narayanan, K., Makino, S., 2012. Roles of the coding and noncoding regions of rift valley Fever virus RNA genome segments in viral RNA packaging. J. Virol. 86, 4034–4039.

Nakabayashi, H., Taketa, K., Miyano, K., Yamane, T., Sato, J., 1982. Growth of human hepatoma-cell lines with differentiated functions in chemically defined medium. Cancer Res. 42, 3858–3863.

Naslund, J., Lagerqvist, N., Lundkvist, A., Evander, M., Ahlm, C., Bucht, G., 2008. Kinetics of Rift Valley fever virus in experimentally infected mice using quantitative real-time RT-PCR. J. Virol. Methods 151, 277–282.

Pepin, M., Bouloy, M., Bird, B.H., Kemp, A., Paweska, J., 2010. Rift Valley fever virus (Bunyaviridae: Phlebovirus): an update on pathogenesis, molecular epidemiology, vectors, diagnostics and prevention (Bunyaviridae: phlebovirus): an update on pathogenesis, molecular epidemiology, vectors, diagnostics and prevention. Vet. Res. 41, 61.

Peters, C.J., Liu, C.T., Anderson Jr, G.W., Morrill, J.C., Jahrling, P.B., 1989. Pathogenesis of viral hemorrhagic fevers: Rift Valley fever and Lassa fever contrasted. Rev. Infect. Dis. 11 (Suppl 4), S743–S749.

Peyrefitte, C.N., Pastorino, B., Bessaud, M., Tolou, H.J., Couissinier-Paris, P., 2003. Evidence for in vitro falsely-primed cDNAs that prevent specific detection of virus negative strand RNAs in dengue-infected cells: improvement by tagged RT-PCR. J. Virol. Methods 113, 19–28.

Plaskon, N.E., Adelman, Z.N., Myles, K.M., 2009. Accurate strand-specific quantification of viral RNA. PLoS One 4 e7468.

Rolin, A.I., Berrang-Ford, L., Kulkarni, M.A., 2013. The risk of Rift Valley fever virus introduction and establishment in the United States and European Union. Emerg. Microbes Infect. 2 e81.

Strydom, E., Pietersen, G., 2018. Development of a strand-specific RT-PCR to detect the positive sense replicative strand of Soybean blotchy mosaic virus. J. Virol. Methods 259, 39–44.

Sun, Y., Li, J., Gao, G.F., Tien, P., Liu, W., 2018. Bunyavirales ribonucleoproteins: the viral replication and transcription machinery. Crit. Rev. Microbiol. 44, 522–540.

Terasaki, K., Makino, S., 2015. Interplay between the virus and host in Rift Valley fever pathogenesis. J. Innate Immun. 7, 450–458.

Tuiskunen, A., Leparc-Goffart, I., Boubis, L., Monteil, V., Klingstrom, J., Tolou, H.J., Lundkvist, A., Plumet, S., 2010. Self-priming of reverse transcriptase impairs strand-specific detection of dengue virus RNA. J. Gen. Virol. 91, 1019–1027.

Vashist, S., Urena, L., Goodfellow, I., 2012. Development of a strand specific real-time RT-qPCR assay for the detection and quantitation of murine norovirus RNA. J. Virol. Methods 184, 69–76.

Wichgers Schreur, P.J., Kortekaas, J., 2016. Single-molecule FISH reveals non-selective packaging of Rift Valley fever virus genome segments. PLoS Pathog. 12 e1005800.

Wilson, W.C., Romito, M., Jasperson, D.C., Weingartl, H., Binepal, Y.S., Maluleke, M.R., Wallace, D.B., van Vuren, P.J., Paweska, J.T., 2013. Development of a Rift Valley fever real-time RT-PCR assay that can detect all three genome segments. J. Virol. Methods 193, 426–431.